# Combining Active Surfaces and Fuzzy Labels for Cortical Functional Activation Mapping

Karin Engel[1], Klaus Toennies[1] and André Brechmann[2]

[1]Otto von Guericke University Magdeburg, Germany, [2]Leibniz Institute for Neurobiology Magdeburg, Germany

**Abstract.** Surface–based representations of the cortex become more and more popular for brain mapping, because they can overcome the topological deficiency of commonly used volume–based methods. The projection of functional volumes onto cortical surface meshes is an essential problem that is, however, rarely studied. This paper presents a method that uses separable, anatomy–based convolution kernels and maps the 3d–functional activations of the regional grey matter volume more precisely onto the cortical surface. To overcome limitations in segmentation accuracy, we use an Active Surface for estimating the center of grey matter based on a fuzzy tissue classification with automatic segmentation as initialisation. Experimental results are presented with data from an auditory fMRI experiment, and indicate that the proposed center–of–grey matter method provides a more accurate cortical functional mapping compared with current techniques.

## 1 Introduction

For identifying brain regions of specific functionality, e.g. using functional magnetic resonance imaging (fMRI), surface–based representations of the cortex become more and more popular. The cortex–based analysis of fMRI data offers several advantages over volume–based analysis methods. For example, statistical analysis methods can benefit from the exclusion of non–cortical signals [1, 2], e.g. signals from the white matter and cerebrospinal fluid (CSF). A cortical surface model that represents the inner, grey–white matter boundary in terms of a polygonal mesh with spherical topology, also allows for a better visualisation and analysis of the spatial extent of activation foci and their locations in group data [3, 4]. There are two frequently used approaches to map the functional activation within the cortical grey matter onto the inner cortical surface. The first method either maps the activation peak between the surfaces to the mesh vertices [5–7], or averages the responses between the inner and outer cortical surfaces [1, 8][1]. The second method employs the center of normal (CN) and assigns to each vertex the value of its containing voxel, and averages signals inside a sphere centered at each vertex of an estimated medial surface within the grey matter, respectively [3, 7, 9, 10][2]. A few methods try to embed explicit anatomical information into the mapping process. The region of influence of each each vertex is defined by the voxels distances to and along this surface, using nearest neighbour averaging [5], 3-dimensional Gaussian kernels with different kernel sizes [2] and 2-dimensional diffusion or heat kernel smoothing [8, 11, 12].

All these methods require accurate segmentation that still require manual corrections to prevent an erroneous mapping of non–cortical signals. Partial volume effects and artefacts due to magnetic field inhomogeneities and noise, however, complicate the segmentation of the cortex from MR images. Automatic methods that separate the grey and white matter brain regions based on intensity histograms require several pre–processing (e.g. an inhomogeneity correction) and post–processing steps (e.g. a correction for topological errors) to produce acceptable results [13]. Methods that employ active contours impose smoothness constraints to the extracted cortical surfaces [14], and thus may fail in highly curved regions, e.g. at the fundus of sulci. Hence, the manual correction of segmentation errors is still the most important, but operator–dependent and time–consuming preprocessing step in view of cortical mapping [2, 10]. This motivates our approach to computing medial surfaces that optimally represent the center of the cortical grey matter.

## 2 Mapping Functional Volumes Onto the Cortical Surface

Similar to the classical CN method, our method uses estimates of the inner, grey–white matter interface and outer cortical surface (where grey matter borders CSF). Instead of improving the surfaces to fit the true boundaries of the cortex, the medial surface initially centered between the two estimates is subsequently deformed to directly find the center of grey matter. It is therefore implemented as an Active Surface that adapts to local maxima in grey matter probability maps, which are obtained by a fuzzy region growing [15]. The fitted surface finally represents the center of grey matter containing the fMRI signals of interest. Our algorithm directly computes the final response at each vertex of the deformed surface by an anatomically–based convolution in the columnar direction and along the surface, i.e. in the laminar direction [1, 11].

[1]The two–surfaces mapping is used in the SUMA software package (`http://afni.nimh.nih.gov/afni/suma`).

[2]The center–of–normal method is used in the Freesurfer software package (`http://surfer.nmr.mgh.harvard.edu/`).

### 2.1 The Center–of–Grey–Matter Surface Model

Input to our method are the inner and outer cortical surfaces obtained from T1–weighted anatomical MR data sets using the popular commercial software package Brainvoyager QX (`http://www.brainvoyager.com`). The grey–white–matter boundaries $\mathbf{V}_W = \{\varphi_i^W\}$ and their inflated versions, representing the outer cortical surfaces $\mathbf{V}_O = \{\varphi_i^O\}$, are smoothed and corrected for topological errors [13], but usually underestimate the included grey and white matter regions [14]. There are several approaches to locate the true cortical boundaries based on initial estimates, e.g. by shifting the surfaces in the CSF direction [10], or deforming the surfaces in the direction of high image gradients [16]. In [15] we proposed method that determines for each voxel the probability of being included into the grey matter region of the individual brain. It uses a multi–scale analysis to make the segmentation of the grey matter less sensitive to noise and weak borders between the adjacent white matter and CSF. The resulting volumetric maps $\mathbf{P}_\rho$ of fuzzy labels are used here to directly estimate the center–of–grey–matter surface $\mathbf{V}_\rho$ in each data set.

The initial vertex positions of the medial surface $\mathbf{V}_\rho^0 = \{\varphi_i^0\}$ are defined as follows. Profile lines of length $\max(\vartheta, \varphi_i^O - \varphi_i^W)$ are drawn through the corresponding vertices $i$ in the inner and outer surfaces, and $\varphi_i^0$ is located at the bisection point. Here, $\vartheta = 3mm$ estimates the average cortical thickness [17]. The resulting surface is represented as an Active Surface [18]. Its undeformed shape can be understood as a continuous domain $\Omega \subset \mathbb{R}^3$, and its smooth deformation is described by a boundary value partial differential equation that is solved numerically for the unknown displacement field $u(\mathbf{x})$, $\mathbf{x} \in \Omega$. We employ the Finite Element Method yielding an algebraic function that relates the deformed positions $\varphi_i^t = \varphi_i^0 + \mathbf{u}_i(t)$ of all $i = 1, \ldots, N$ finite element nodes (the mesh vertices) to elastic, inertial and damping forces and external forces $\mathbf{f}(t)$. The dynamic equilibrium equation has the form

$$\ddot{\mathbf{u}}(t) = \mathbf{M}^{-1}(-\mathbf{C}\dot{\mathbf{u}}(t) - \mathbf{K}\mathbf{u}(t) + \mathbf{f}(t)), \tag{1}$$

where $\ddot{\mathbf{u}}(t) \approx \frac{\partial^2 \mathbf{u}}{\partial t^2}|_{t>0}$ and $\dot{\mathbf{u}}(t) \approx \frac{\partial \mathbf{u}}{\partial t}|_{t>0}$, and $\mathbf{K}(E, \nu)$ represents the stiffness properties. $\mathbf{C}$ approximates a velocity–dependent damping, and $\mathbf{M}$ is a constant function of material density $\varrho$ [18, 19]. For simulating the deformation of the template, we use a step size $\triangle t$, and integrate the finite element equations (Eq. 1) over time until an equilibrium is reached. The deformed positions constitute the final center–of–grey matter surface $\mathbf{V}_\rho$.

### 2.2 Fit of the Active Surface

The external forces in Equation 1 shall attract the nodes in normal surface direction to the voxels with maximum grey matter probability. In order to avoid drifting of the surface into regions of non–brain tissue, e.g. CSF, we use ratched spring forces according to [19], and let

$$\mathbf{f}_i(t) = \mathbf{f}_i(t-1) + \kappa_s(\varphi_i^{opt} - \varphi_i^t), \qquad \kappa_s > 0. \tag{2}$$

These forces simulate springs, which are tightened until the surface matches the points at which the grey matter probability is high. The locally optimum position for each vertex is computed from the grey matter probability map $\mathbf{P}_\rho$ as

$$\varphi_i^{opt} = v_j : j = \max_{v_j \in X_i} \mathbf{P}_\rho(v_j).$$

The set of voxels $X_i$ is defined in the vicinity of the initial surface $\mathbf{V}_\rho^0$ by sampling along the surface normal profile $(\varphi_i^0 + \vartheta \mathbf{n}_i) - (\varphi_i^0 - o\mathbf{n}_i)$. Here, $\vartheta = 3mm$ and the offset $o = 2mm$ account for possible segmentation errors, and $\mathbf{n}_i$ denotes the average outward surface normal in the initial vertex position.

Similar to the self–proximity term used in [16], an additional force is used to prevent arbitrary self–intersections of the surface and thereby preserve its topology. We compute in each iteration for each vertex $\varphi_i^t$ the nearest (non–adjacent) surface point $\mathbf{x} \in \Omega$ in direction of the velocity of the vertices, and test for a potential collision. If the Euclidean distance between $\varphi_i^t$ and estimated collision point is below a threshold $\theta$, the vertex and collision point are added to a list of "active pairs". For these active vertices we compute the impulse–based collision response in inverse velocity direction as described in [20], and use this force in Equation 1. With this scheme it is possible to parametrise the Active Surface less stiff in order to fit highly curved regions, while avoiding changes in the surface topology due to self–intersections. We let $\theta = \vartheta$ in gyral regions (with positive mean curvature). Since the grey matter is thinner in the fundi of sulci [16, 17], $\theta = 2mm$ in sulcal regions.

### 2.3 Cortical Functional Activation Mapping

According to the columnar architecture of the cortex, we expect homogeneous activity normal to the surface within the cortical ribbon. However, with increasing distance from the medial surface the probability increases that the voxels

partially include signals from non–grey matter or grey matter volume from opposite sides of a fold. Further, the correlation between responses at two surface points depends on their geodesic distance. In accordance with these assumptions, the distribution of activity on the cortical surface is represented as an anatomically–based function of normal and parallel (geodesic) distance to and on the medial surface.

For the columnar smoothing an approximative 1–dimensional Gauss kernel $(g_1 \dots g_n)$ is centered directly at each vertex of the medial surface $\mathbf{V}_\rho$. For each vertex we collect $n$ samples $(s_1 \dots s_n)$ from the fMRI volume along a columnar profile of length $l = \vartheta + 2o_C, o_C = 1mm$, drawn from $\varphi_i^t$ in normal direction to the inner and outer cortical surfaces. The standard deviation $\sigma_C$ of the columnar kernel is a function of local mean curvature. According to the assumption that the cortex has an average thickness of $3mm$, and is less thick in the fundus of sulci [16, 17], we let $\sigma_C = 0.6mm$ in gyral regions with positive mean curvature, and $\sigma_C = 0.3mm$ in sulcal regions. Thereby, the signal is averaged over samples with a maximum distance from the medial surface of about $2mm$ and $1mm$, respectively. The signal assigned to $\varphi_i^t \in \mathbf{V}_\rho$ is then $S(\varphi_i^t) = \sum_{j=1}^{n} s_j g_j$. The following smoothing of the field $S$ along the surface uses a heat diffusion kernel [1, 11], whose weights are calculated based on inter–vertex distances $d_{ij} = |\varphi_i^t - \varphi_j^t|^2$. In our case, the geodesic distances on the folded surface $\mathbf{V}_\rho$ are approximated by the length of the shortest path between the vertices, computed using Dijkstra's algorithm. Assuming a sufficiently small laminar kernel bandwidth $\sigma_L$ and small inter–vertex distances,

$$g(\varphi_i^t, \varphi_j^t) = \frac{\exp(-d_{ij}(2\sigma_L)^{-2})}{\sum_{j=1}^{m} \exp(-d_{ij}(2\sigma_L)^{-2})}. \tag{3}$$

Here, the set $\{\varphi_1^t, \dots, \varphi_m^t\}$ contains $\varphi_i^t$ and the neighboring vertices, whose distance to $\varphi_i^t$ is below a threshold $d_L = 3\sigma_L$. The discrete convolution $g * S(\varphi_i^t) = \sum_{j=1}^{m} g(\varphi_i^t, \varphi_j^t) S(\varphi_j^t)$ is then repeated $t_L$ times to obtain the final mesh time courses $S$.

## 3 Experimental Evaluation

We evaluated the above algorithm using 10 anatomical MR data sets with $(256^3)$ $1mm$ iso–voxels acquired on a 3 Tesla scanner. The quality of the data varied w.r.t. signal–to–noise ratio and intensity inhomogeneities. The cortices were reconstructed using Brainvoyager QX, and the grey matter probability maps were computed as described in [15]. We first analysed the estimated center–of–grey matter surfaces using our technique in comparison with other methods, and finally evaluated the resulting cortical functional maps from data acquired in an auditory fMRI experiment.

The same set of parameters introduced in Section 2 were used for all data sets. We let $E = 2, \nu = 0.4, \rho = 1, \kappa_s = 100$, $\triangle t = 0.05, \vartheta = 3mm, o = 2mm, \theta \in \{2mm, 3mm\}, \sigma_C \in \{0.3mm, 0.6mm\}, o_C = 1mm, n = 20, t_L = 1$ and $\sigma_L = 0.9mm$ (The value for $\sigma_L$ equals the average inter–vertex distance on the surface meshes.).

### 3.1 Center–of–Grey–Matter Estimation

We computed estimates of the medial surface in the center of the cortical grey matter using variants of the CN method, namely using the center between the cortical surfaces (1), shifting the cortical surface mesh $\mathbf{V}_W$ for $\tau = \frac{1}{2}\vartheta$ (2), and $\tau = 2mm$ (3), respectively (similar to, e.g. [10]). We will refer to our Active Surface–based algorithm as method 4.

A visual inspection by neurobiologists suggested that the medial surface found by our algorithm was usually more exact, especially in regions of low contrast, such as the lower temporal lobe. In all cases, the grey matter probability along the deformed surfaces $\mathbf{V}_\rho$ computed using our method was higher compared with the initial estimates $\mathbf{V}_\rho^0$ (Sect. 2.1). The values $\mathbf{P}_\rho(\mathbf{V}_\rho)$ were also significantly higher compared to methods 1-3 ($p < 0.01$, one–sided $t$–test). For a quantitative comparison of the surfaces $\mathbf{V}_\rho$, we restricted our analysis to a portion of the surfaces where a set of manually labelled landmarks was available as ground truth. 20 landmarks were set in each data set by a neuroscientist in the grey matter of the first transverse temporal gyrus (Heschl's gyrus), adjacent Heschl's sulcus, sulcus temporalis superior and planum temporale. The landmarks were placed in regions where the distinction between neighbouring gyri or opposing banks of the sulci has been obscured by partial volume. Our segmentations identified an average absolute distance of $\delta = 0.2 \pm 0.04mm$ and a maximum distance of $d = 1.1mm$ to the ground truth. Since the Brainvoyager segmentations underestimate the white matter, methods 1-3 yielded poor results. Among them, method 3 performed best ($\delta = 1.1 \pm 0.72mm, d = 5.48mm$). We further analysed the overlap of the medial surfaces with segmentations of the grey matter of two regions including the primary auditory cortex and secondary auditory cortex. The grey matter masks were defined as described in [21], and segmented in each MRI data set by an expert. Again, method 4 computed the highest overlap of $96 \pm 1\%$ (method 3: $90 \pm 2\%$, method 2: $87 \pm 2\%$, method 1: $86 \pm 3\%$).

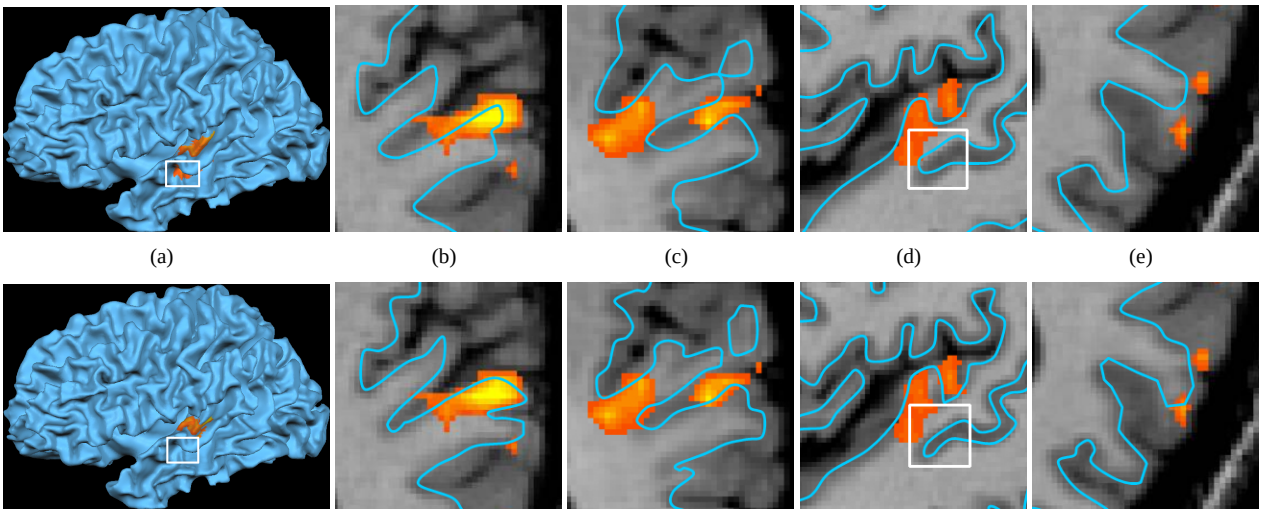


**Figure 1.** Cortical activation maps computed using method 3 (top row) and the proposed Active Surface (bottom row). Using our method, the number of missed activations was smaller (compare Figs. (e) and (j)). The resulting maps were also topologically more accurate. In contrast to Fig. (f) the map in (a) shows activations on the superior temporal sulcus (indicated by the box) due to an erroneous mapping of fMRI signals from the superior temporal gyrus. In this example, a fix shift of the inner cortical surface produced a medial surface that intersects the white matter (Fig. (d)). The Active Surface deformed more precisely into the grey matter of the sulcus (Fig. (i)). As a result, the distance of the medial surface to the activation in the superior temporal gyrus increased.

Our algorithm explicitly accounts for self–intersections by employing a collision handling (Sect. 2.2). As a result, less than $0.01\%$ vertices of each deformed surface had a normal distance below $\vartheta$ to the surface. These vertices were located in both gyral and sulcal regions, where the contrast between CSF and grey matter was low. No self intersections were identified (Fig. 1(h)). Such topological changes occurred in a second experiment, where we calculated the deformation of the Active Surface without the collision handling. In one data set, where the white matter was overestimated by the commercial software package, $0.02\%$ vertices intersected the deformed surface. For this data set we found similar results using method 3.

### 3.2 Cortical Mapping using the Center–of–grey matter

Detection of activations were made vertex–wise based on the mesh time courses $S$ (Sect. 2.3), implemented by the same deconvolution–based techniques commonly used in volume–based analysis. Because no ground truth was available, we compared the resulting cortical activation maps with the maps obtained using the medial surfaces computed estimation method 3, which produced the best CN method–based estimates for the medial surface (Sect. 3.1). In order to examine the topological accuracy of the maps we compared the 3d–activation foci w.r.t. their counterparts on the surfaces. For the volume–based analysis, the fMRI volumes were smoothed using a 3-dimensional isotropic Gaussian kernel with $2mm$ full width at half maximum (FWHM)[3].

From Section 3.1 we can conclude that the probability of mapping non–grey matter signals to the surfaces was reduced using our algorithm. A visual inspection of the cortical maps also showed differences between our method and method 3 w.r.t. the probability of mixing signals from different grey matter regions to the vertices. Method 3 computes the location of the medial cortical surface based on a fix shift of the inner cortical surface in normal direction. Some 3d–activations were missed, because the inner cortical surface had not always a fix distance of $2mm$ to the true grey–white matter boundary (Figs. 1(b), 1(e)). Further, in some cases, method 3 assigned clusters of activation to cortical locations that did not correspond with the specific anatomical location assigned by evaluating its location using the 3d–statistical volume. For example, clusters were "multiplied" and assigned to different sides of folds, which were close in an Euclidean sense, but geodesically distant (Figs. 1(a), 1(d)). We found no evidence for such erroneous mappings using the proposed Active Surface–based method (Figs. 1(f), 1(i)).

[3]For the chosen values $\sigma_L = 0.9mm$ and $t_L = 1$ (used to map the fMRI volumes to the surfaces), the predicted FWHM Gaussian filter width is slightly higher ($2.2mm$) [11]. Larger values may be chosen for multi–subject statistical analyses, but increase partial volume effects. As a result, separate clusters of cortical activation may fuse into one cluster.

## 4 Conclusion and Outlook

We presented an automatic procedure for estimating the center–of–grey–matter surface based on the reconstructed inner and outer cortical surfaces provided by a commercial software package. The pre–defined surfaces usually underestimate the true boundaries of the cortex. To overcome the segmentation errors as much as possible, our method employs smoothness constraints on a medial surface, which is deformed from its initial location to match the maxima in grey matter probability maps. An additional constraint helps to avoid self–intersections when fitting the surface to thin folds. The resulting medial surfaces provide more accurate estimates of the true center of grey matter and of the cortical functional activation maps computed using the popular center–of–normal method. Our results also compare well with the interpretation of 3d–activation patterns by neuroscientists. By these considerations, the proposed technique can support the cortical analysis of fMRI data. Currently, our method for practical applications needs more detailed evaluation, e.g. using synthetic and real MRI data of different spatial resolution. Future work will focus on the analysis of the influence of the parameters on the resulting medial surfaces, e.g. the influence of the curvature–dependent smoothing kernel width on partial volume effects. We will also evaluate the potential of the Active Surface to compensate larger differences between the given surfaces and true boundaries of the cortex.

## References


1. Andrade A., et al.: Detection of fMRI activation using cortical surface mapping. *Human Brain Mapping* **12** (2001) 79-93
2. Kiebel S., et al.: Anatomically informed basis functions. *Neuroimage* **11** (2000) 656-667
3. Fischl B., et al.: High–resolution inter–subject averaging and a coordinate system for the cortical surface. *Human Brain Mapping* **8** (1999) 272–284
4. Operto G., et al.: Surface–based structural group analysis of fMRI data. *Proc. MICCAI* (2008) 959–966
5. Desai R., et al.: Volumetric vs. surface–based alignment for localization of auditory cortex activation. *Neuroimage* **26** (2005) 1019–1029
6. Hagler D., et al.: Smoothing and cluster thresholding for cortical surface-based group analysis of fMRI data. *Neuroimage* **33** (2006) 1093-1103
7. Saad, Z., et al:. Suma: an interface for surface-based intra- and inter-subject analysis with AFNI. *Proc. IEEE ISBI* 1510
8. Operto G., et al.: Projection of fMRI data onto the cortical surface using anatomically-informed convolution kernels. *Neuroimage* **39** (2008) 127-135
9. Jo H., et al.: Spatial accuracy of fMRI avtivation influenced by volume- and surface-based smoothing techniques. *Neuroimage* (2007) 550–564
10. Warnking J., et al.: fMRI retinotopic mapping. *Neuroimage* **17** (2002) 1665-1683
11. Chung M., et al.: Cortical thickness analysis in autism with heat kernel smoothing. *Neuroimage* **25** (2005) 1256-1265
12. Grova C., et al.: Anatomically informed interpolation of fMRI data on the cortical surface. *Neuroimage* **31** (2006) 1475-1486
13. Kriegeskorte N. and Goebel R.: An efficient algorithm for topologically correct segmentation of the cortical sheet in anatomical MR volumes. *Neuroimage* **14** (2001) 329-346
14. Sokoll S., et al.: Dynamic segmentation of the cerebral cortex in MR data using implicit active contours. *Proc. MIUA* (2008) 184–188
15. Engel K., et al.: Fuzzy Multiscale Region Growing for Segmentation of MR Images of the Human Brain. *Proc. BVM* (2009) 242–246
16. MacDonald D., et al.: Automated 3-D extraction of inner and outer surfaces of cerebral cortex from MRI. *Neuroimage* **12** (2000) 340–356
17. Fischl B. and Dale A.: Measuring the thickness of the human cerebral cortex from magnetic resonance images. *Proc. Nat Acad Sci* **97** (2000) 11044–11049
18. Cohen L. and Cohen I.: Finite-element methods for active contour models and balloons for 2-D and 3-D images. *IEEE Trans Patt Anal Mach Intell* **15** (1993) 1131-1147
19. Sclaroff S. and Pentland A.: Modal matching for correspondence and recognition. *IEEE Trans Patt Anal Mach Intell* (1995) **17** 545-561
20. Baraff D. and Witkin A.: Dynamic simulation of non-penetrating flexible bodies. *Proc. SIGGRAPH* (1992) 303–308
21. Brechmann A., et al.: Sound–level–dependent representation of frequency modulations in human auditory cortex: A low noise fMRI study. *J Neurophysiology* **87** (2002) 423–433